GEOPHYSICS, VOL. 76, NO. 4 (JULY-AUGUST 2011); P. B139–B150, 11 FIGS.
10.1190/1.3581358

Case History

Quantitative interpretation for gas hydrate accumulation in the eastern Green Canyon Area, Gulf of Mexico using seismic inversion and rock physics transform

Zijian Zhang[1], De-hua Han[2], and Qiuliang Yao[2]

ABSTRACT

Gas hydrate can be interpreted from seismic data through observation of bottom simulating reflector (BSR). It is a challenge to interpret gas hydrate without BSR. Three-dimensional qualitative and quantitative seismic interpretations were used to characterize gas hydrate distribution and concentration in the eastern Green Canyon area of the Gulf of Mexico, where BSR is absent. The combination of qualitative and quantitative interpretation reduces ambiguities in the estimation and identification of gas hydrate. Sandy deposition and faults are qualitatively interpreted from amplitude data. The 3D acoustic impedance volume was interpreted in terms of high P-impedance hydrate zones and low P-impedance free gas zones. Gas hydrate saturation derived from P-impedance is estimated by a rock physics transform. We interpreted gas hydrate in the sand-prone sediments with a maximum saturation of approximately 50% of the pore space. Sheet-like and some bright spot gas hydrate accumulations are interpreted. The interpretation of sheet-like gas hydrate within sand-prone sediments around faults suggests that fluid moves into the sand zones laterally by conduits. Variations in depths of interpreted gas hydrate zones imply nonequilibrium conditions. Low P-impedance free gas zones within high P-impedance gas hydrate zones imply possible coexistence of hydrate and free gas within the hydrate stability zone. We propose that gas hydrate distribution and concentration are associated with structures, buried sedimentary bodies, sources of gas, and fluid flux.

INTRODUCTION

Gas hydrates are ice-like solids composed of gas molecules enclosed in cages of water molecules. They occur in marine sediments along continental margins (Kvenvolden and Barnard, 1982). It is important to understand the seismic properties of gas hydrate because of its potential as a future energy resource, a drilling hazard, and a submarine geologic hazard (Kvenvolden, 1998).

The occurrence of gas hydrate can be detected by observing the bottom simulating reflector (BSR) from seismic data (Markl et al., 1970). The BSR is often located at the base of the gas hydrate stability zone, as the result of an impedance contrast between gas hydrate-bearing sediment and free gas trapped in the sediment underneath the gas hydrate. Numerous researchers have interpreted and analyzed gas hydrate in various geologic environments, where the BSR is visible (Andreassen et al., 1995, 1997; Yuan et al., 1996, 1999; Ecker et al., 1998; Lu and McMechan, 2002; Tréhu et al., 2004; Zhang and McMechan, 2006). In the Gulf of Mexico, however, the abundant continuous BSRs are much less present than in other areas (Cooper and Hart, 2002). To identify gas hydrate in an area without BSRs is difficult.

Fluid migration is a relatively common process in the deep marine environment. Mud volcanoes, seafloor mounds, pockmarks, gas hydrate, and chimneys are possible products of the

Manuscript received by the Editor 19 August 2010; revised manuscript received 28 November 2010; published online 10 June 2011.
[1]University of Houston, Department of Earth and Atmospheric Sciences, Rock Physics Lab, Houston, Texas, U.S.A. and AOA Geophysics, Inc., Houston, Texas, U.S.A. E-mail: zijian1616@gmail.com.
[2]University of Houston, Department of Earth and Atmospheric Sciences, Rock Physics Lab, Houston,, Texas, U.S.A. E-mail: dhan@uh.edu; qiuliang.yao@mail.uh.edu.

fluid migration. However, the process is not well understood. Fluid migration is not only associated with faults and salt, but also sand-prone deposits and erosion surfaces. Fluid migration is much more effective in faults, salt diapirs, or unconformities than a simple diffusive seepage through the sedimentary column (Abrams, 1992; Brown, 2000). Faults acting as main pathways for fluid migration in the Gulf of Mexico have been described (Reilly et al., 1996). Gas hydrate occurs on the seafloor and near seafloor, indicating that gassy fluids move into the gas hydrate stability zone. One objective of this study is to understand the relation between fluid pathways and gas hydrate.

Highly concentrated gas hydrate has been drilled in the unconsolidated sandy deposits at Mallik 2L-38 well in the Arctic in 1998 (Dallimore et al., 1999). Recent studies suggest highly concentrated gas hydrate exists within coarse-grained sandy deposits in marine environments in offshore Vancouver (Expedition 311 Scientists, 2006) and the Gulf of Mexico (Boswell et al., 2009). Scientists in Gulf of Mexico Gas Hydrate Joint Industry Project (JIP) suggest a concept of gas hydrate petroleum systems to identify the occurrence of gas hydrate in coarse-grained sandy deposits (Hutchinson et al., 2008; Jones et al., 2008). The concept emphasizes the presence of sand-prone deposits within the gas hydrate stability zone, a gas source close to the deposits, and a migration pathway that can transport gas into the deposits (Ruppel et al., 2008).

Our study area is in the Green Canyon (GC) blocks 473 and 474, Gulf of Mexico. We present a method of integrated seismic interpretation, both qualitative and quantitative, to predict gas hydrate reservoirs in sand-prone deposits by seismic amplitude interpretation, seismic inversion, and rock physics-based gas hydrate prediction. We first detected the sand-prone sequences by qualitative seismic interpretation. Then, we estimated the high P-impedance, indicating gas hydrate, and low P-impedance, indicating free gas, within the sand-prone sequences by acoustic inversion. Finally, we estimated the gas hydrate saturation based on the rock physics model. Qualitative seismic interpretation provides the structure and stratigraphy information of the area. Quantitative seismic interpretation presents the elastic properties of the sand-prone sediments with gas hydrate and free gas.

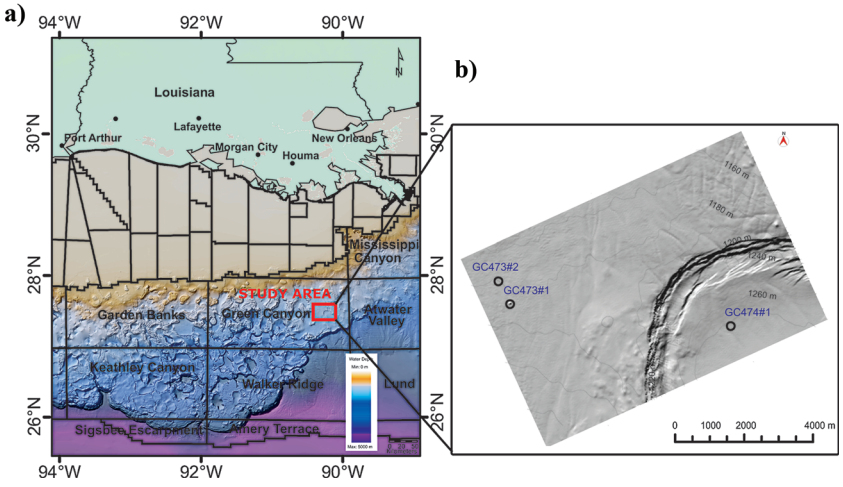

Figure 1. (a) Location of Green Canyon. (b) The 3D seismic survey and three wells represent the inset in (a). The seafloor rendering is computed from seafloor picking of 3D seismic data and illustrates seafloor fault scarps and seafloor mounds in the vicinity of the fault scarps. Contours are at 10-m intervals of water depth. The black circles are the wells of GC473 #1, GC473 #2, and GC474 #1.

THE STUDY AREA

Geologic setting

The study area is in the eastern Green Canyon on the upper continental slope of Texas and Louisiana, where near-surface geology is dominated by active salt tectonics and rapid sea level-driven sedimentation (Figure 1). Salt diapirs are common on the upper slope. The mobile salt has extensively fractured the overlying sediments with regional growth faults and associated fault types. These faults act as conduits for the migration of hydrocarbons from deep layers to shallow sections.

Gas hydrate has been found in the northern Gulf of Mexico for years. In 1984, Brooks et al. (1984) discovered gas hydrate in the near-surface sediments from piston cores in the Green Canyon. The Deep Sea Drilling Project (DSDP) collected gas hydrate from 20 to 40 m below seafloor at site 618 in Orca Basin (Pflaum et al., 1986). JIP identified gas hydrate from logging data with high anomalies of resistivity and velocity in the Green Canyon and Walker Ridge (Boswell et al., 2009). In addition to gas hydrate, oil and gas seeps have been observed on the seafloor in the Gulf of Mexico (MacDonald et al., 1989; Sassen et al. 1999a,b). Sassen et al. (2001) illustrate a belt of gas hydrate, oil and gas seeps with chemosynthetic communities, and oil fields across the Green Canyon. Our study area is located within the southern portion of this belt.

The terrigenous coarse-grained sediments were delivered and mainly deposited onto the upper continental slope in our study area in the form of turbidite deposits during sea level lowstands. Channels and fan lobes may be present in the period (Mann et al., 1992). During periods of sea level highstands, fine-grained sediments formed thin hemipelagic and pelagic layers in the area (Mann et al., 1992). The occurrences of shallow water flow sand during drilling in the northeastern Green Canyon suggest sandy sediments and fast sediment accumulation rates during the late Pleistocene in the area (Ostermeier et al., 2002).

Prediction of the hydrate stability zone

Free gas can be stable as a solid gas hydrate under the conditions of high pressure and low temperature. We estimate the conditions using the CSMHYD hydrate program (Sloan, 1998). The base of the hydrate stability zone is also controlled by salinity. Normal salinity in the Gulf of Mexico is about 3.5% (Milkov and Sassen, 2002), but it can be quite high on active seeps and/or near salts. Figure 2 illustrates the gas hydrate stability curves of both 3.5% and 8% NaCl for a gas composition of 100% methane. Geothermal gradients in deepwater range from 10°C/km to 25°C/km in the central Gulf of Mexico (Milkov and Sassen, 2002), but the geothermal gradients could be locally higher in some areas near faults with fluid flows. Forrest et al. (2005) estimate a geothermal gradient of

15°C/km in the Green Canyon area. The constant geothermal gradients of 15°C/km to 30°C/km are shown in Figure 2. Assuming the bottom water temperature of 4.4°C, we expect that the base of the gas hydrate stability zone to range from approximately 280 to 880 m below mudline (BML) in the area.

Data set and well information

This study used a poststack Kirchhoff time-migrated 3D seismic volume. The data were processed for hydrocarbon exploration purposes and are suitable for a shallow gas hydrate study. The frequency of the seismic data in the shallow section ranges from 40 to 60 Hz. Inlines are spaced 40 m (131.2 ft) apart; crosslines are spaced 25 m (81.02 ft) apart.

Offset well control in the area includes GC473 #1 and GC474 #1. Checkshots from well GC473 #1 were used to build a subsurface depth conversion function. Well logs from wells GC473 #1 and GC474 #1 were available for the study. The wells log measurements include velocity, density, porosity, resistivity, and gamma ray. The measurements for velocity, density, resistivity, and gamma ray start at approximately 640 m BML in the GC473 #1 well; porosity starts at 975 m BML (Figure 3). The velocity and porosity profiles in shallower sections are extrapolated by empirical shale trends for the shallow sediments in the Gulf of Mexico. The density profile shallower than 640 m BML is computed from the porosity trend of shale. No well logs for GC474 #1 were recorded in the shallow depths.

QUALITATIVE INTERPRETATION

Water depths range from 1160 m in the northeast to 1270 m in the southeast, generally increasing to the south. Large arcuate faults are downthrown to the south and the east and have offsets from 15 to 30 m (Figure 1b). A crossline profile on the south of the survey illustrates the normal master fault that intersects the seafloor (fault A in Figure 4b). The arcuate faults form a salt withdrawal basin in the east. Seafloor mounds are located to the west and north of the faults (Figures 1 and 5). A wipe-out zone under the mounds indicates possible fluid migration upward to the seafloor (Figure 5). These mounds are interpreted to be authigenic carbonate mounds or hydrate mounds.

For the purpose of description, we assigned three depositional sequences. The mapped horizons and sequences have no special significance other than the fact that sequence boundaries are relatively continuous reflections throughout the study area. The boundary between sequences 2 and 3 indicates the base of channels. Figure 4a and 4b depicts a seismic inline and a crossline showing the shallow stratigraphy.

Sequence 1 consists of two distinct depositional sections (Figure 4). The upper section is parallel to the seafloor and contains continuous reflectors representing clay-prone hemipelagic drape. The lower section is a low-amplitude acoustically chaotic section that is interpreted to represent thick clay-prone submarine landslide deposits. The thickness of the landslide deposits ranges from 145 m in the northwestern corner to 390 m in the minibasin in the southeastern study area. The landslide deposits indicate rapid sedimentation in the area.

The seismic characteristics of sequence 2 are different from those of sequence 1, and they are composed of moderate-to-high amplitude, chaotic seismic reflections on the upper section interpreted to represent predominately clay-filled debris flow deposits possibly interbedded with silts and sands (Figure 4). The lower section of the sequence is characterized by complex channel systems (Figure 4b). The channel system displays low-to-high amplitude, irregular reflection facies. In Figure 6, a 3D amplitude map at 0.4 s below seafloor indicates the channel system trending north-south in the western part and a possible slope fan in the eastern part. Over the extent of the study area, the width of the channel system ranges from 2250 to 4200 m. The seismic characteristics suggest sand-prone sediments within the lower section.

Channel systems and lobes are relatively common in sequence 3. The sequence is divided into upper, middle, and lower sections. The upper section is characterized by a low-to-moderate amplitude, locally discontinuous reflection interpreted to represent clay-prone landslide deposits possibly interbedded with sands (Figure 4). The middle section is interpreted as sand-prone

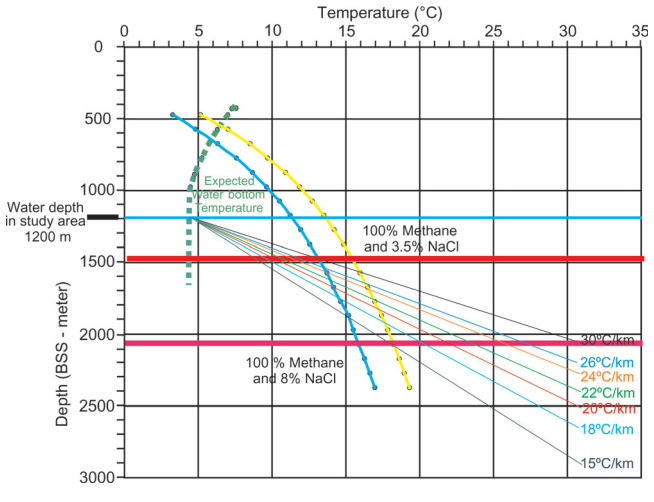

Figure 2. Gas hydrate equilibrium for 100% methane with 3.5% NaCl and 8% NaCl intersecting with geothermal gradients shows the possible gas hydrate stability zone. The equilibrium calculation is from the CSMHTD program (Sloan, 1998).

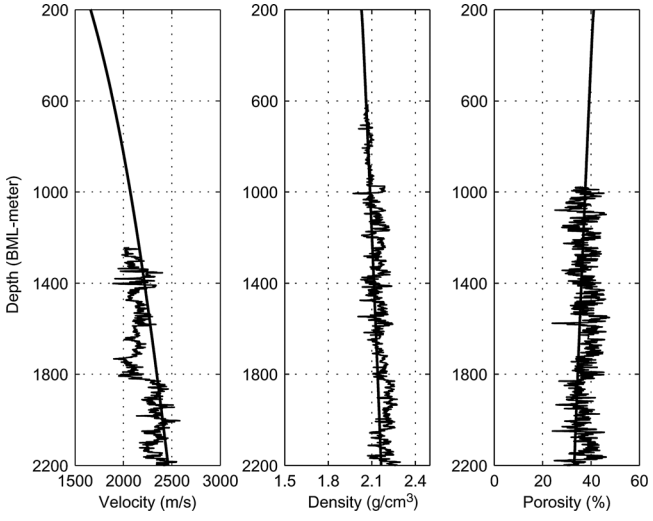

Figure 3. Velocity (P-wave), density, and porosity log from the GC473 #1 well. The solid lines are extracted from the well data by the empirical depth trends.

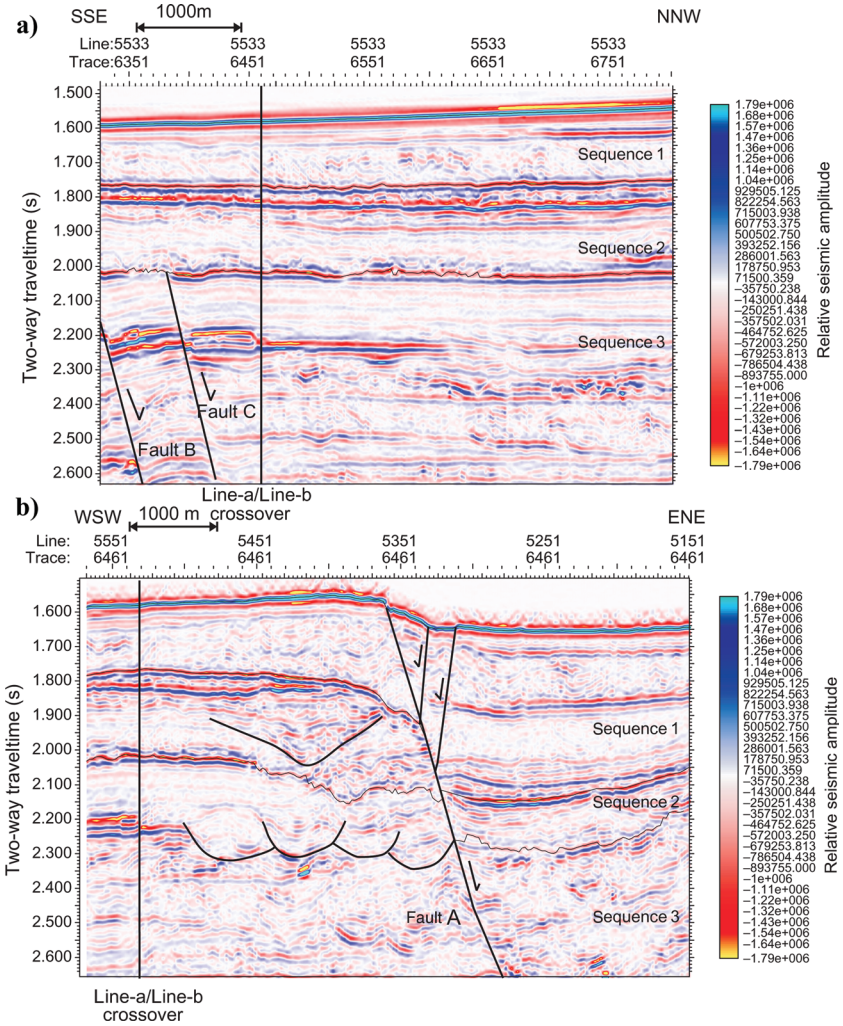

Figure 4. Three-dimensional seismic inline profile (a) and crossline profile (b). The interpreted sequence 1, sequence 2, and sequence 3 are labeled. The black solid lines are interpreted as faults. Fault A is a seafloor fault. Faults B and C are buried faults and cut possible sand-prone sediments between 2.2-s TWT and 2.3-s TWT. Interpreted channels are shown in (b).

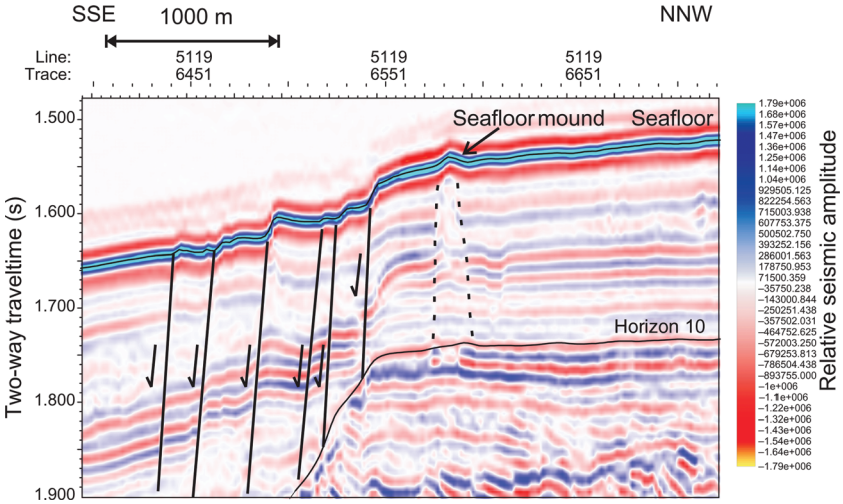

Figure 5. Seismic image illustrates a seafloor mound. Dashed lines delineate the expulsion feature of the seafloor mound in the seismic section. Note the continuous reflectors in horizon 10 and the chaotic zones beneath the mound.

channel and channel lobe deposits (Figure 4). The low-to-moderate amplitude, irregular reflections in the northwestern part of the study area (Figure 4b) may represent channel fill or levee deposits, whereas the moderate-to-high amplitude, parallel reflections in the southwestern part of the study area (Figure 4a) probably indicate channel lobe deposits. The interpretation is supported by information from the GC473 #2 well (Figures 1 and 6) that shallow sand was reported in the Bureau of Ocean Energy Management, Regulation and Enforcement (BOEMRE) database (2010). The lower section is interpreted as low-amplitude mass transport deposits.

We interpreted possible free gas by identifying the anomaly of high negative amplitude and bright spots from 3D seismic data. The interpreted gas is generally within the window of the bottom of the gas hydrate stability zone from 230 to 820 m BML. No high amplitude anomalies interpreted to be free gas are found in sequence 1. The free gas interpreted from these anomalies is associated with channel deposits and/or fault traps in sequences 2 and 3. Classic BSR is a negative continuous reflection parallel to the seafloor. McConnell and Kendall (2002) indicate an interpreted BSR that is a number of bright spots from different reflections parallel to the seafloor in the Gulf of Mexico. Neither a classic nor an interpreted BSR was found in the area. A detailed interpretation of the absence of BSR is discussed below.

Two large normal faults are clearly shown in the western part of the study area from the inline profile (faults B and C in Figure 4a). These faults generally trend to the northwest and are downthrown to the northeast. The presence of these faults is very important for the vertical migration of free gas. These faults are formed in response to salt movement. Seismic data shows salt cut across gas-filled sand intervals at approximately 4000 m below sea surface (BSS). The evidence indicates that salt and faults serve as conduits for gas migrating upward. The tops of these buried faults are located in the base of sequence 2 at approximately 2-s two-way traveltime (TWT; ~360 m BML). These buried faults cut sand-prone channel levee deposits at approximately 2.3-s TWT (~520 m BML) in the middle part of sequence 3. High-amplitude anomalies interpreted to be shallow gas suggest that free gas has migrated laterally into the sand-prone deposits. The sand-prone deposits are located within the computed base hydrate stability zone. In Figure 4a, the seismic response of local high positive amplitude over high negative amplitude in the deposits could indicate high-impedance gas hydrate over low-impedance free gas.

QUANTITATIVE INTERPRETATION

Gas hydrate estimation

We perform a two-step approach to estimate the gas hydrate. First, we invert for acoustic impedance through seismic inversion. Then, we estimate the gas hydrate saturation from the acoustic impedance (P-impedance) using a rock physics model of gas hydrate.

Rock physics depth trends

Understanding the expected depth trends in rock physics properties can reduce the uncertainties in gas hydrate estimation. In addition, these depth trends are crucial in estimating a low-frequency model for seismic inversion in very shallow areas, where well log data are not available. In general, acoustic impedance increases with depth, due to compaction and porosity reduction. Dutta (2009) derives empirical compaction depth trends for the shallow sediments in the Gulf of Mexico by integrating in situ logging data in the Green Canyon, the laboratory measurements, and core data provided by Gregory (1977) and Hamilton (1979). Given the porosity and velocity constraints in the deep sections, we modified the empirical parameters of the trends to obtain our porosity trend,

$$\varphi = 0.2875e^{-0.00774z} + 0.4083e^{-0.00003261z}, \quad (1)$$

and velocity trend,

$$V_P = 6618e^{0.00002963z} - 1652e^{-0.0003646z}. \quad (2)$$

In equations 1 and 2, φ is the porosity in fraction, V_P is the velocity in ft/s, and z is the depth below seafloor in feet.

The porosity of clays is expected to vary from 41% at 200 m BML to 37% at 820 m BML within the interested gas hydrate occurrence zone; the porosity of sands would vary from 39% to 37% in the same area. We assume that no anomalously higher porosity than normal trend and anomalously higher pore pressures are present in the sandy sediments in the study area. We made this assumption because there are no shallow water flow events suggesting high pressure sands in the GC473 #1 and GC474 #1 wells, and the GC473 #2 well is a shallow-water-flow-sand well, but no flow was reported (BOEMRE, 2010).

Seismic inversion

We performed a trace-based inversion for acoustic impedance using linear programming sparse spike inversion with Hampson-Russell's software. The inversion finds acoustic impedance by minimizing the objective function that is a combination of the reflection coefficient and seismic fit. The function is given as (Li, 2001)

$$J(m) = \sum_{n=0}^{N-1} |r_n| + |Lm - d| \quad (3)$$

where r_n is the reflection coefficient of the model, L is the linear operator, m is the model data, and d is the actual seismic data. Such seismic inversion for gas hydrate characterization in shallow unconsolidated sediments has been used by Lu and McMechan (2002), Dev and McMechan (2010), and others.

The low-frequency impedance trend is not present in the seismic data. It is usually derived from well logs or a seismic velocity model. We have neither V_P nor density log in the shallow section. Therefore, we estimated the low-frequency V_P and density from the empirical depth trend and check shots data, calibrated with deeper well logs from wells GC473 #1 and GC474 #1. The wavelet is defined by finding the best match between the real seismic data and the synthetic data computed by convolving well log reflection coefficients with the source wavelet.

Rock physics transform between acoustic impedance and gas hydrate saturation

Rock physics analysis can provide the relationship between the seismic parameters (V_P, density, and P-impedance) and sediment parameters (porosity and hydrate saturation). Under the situation of normal compaction, the relation between acoustic impedance and porosity for the clay baseline can be established from the rock physics depth trend. A smooth baseline curve shows that porosity decreases and impedance increases with increasing depth. The impedance derived from the smooth baseline is defined as background impedance. We divide shallow sediments into water-saturated sediments, hydrate-saturated sediments, and gas-saturated sediments. At any given depth, the sum of water, gas hydrate, and free gas volume fractions is

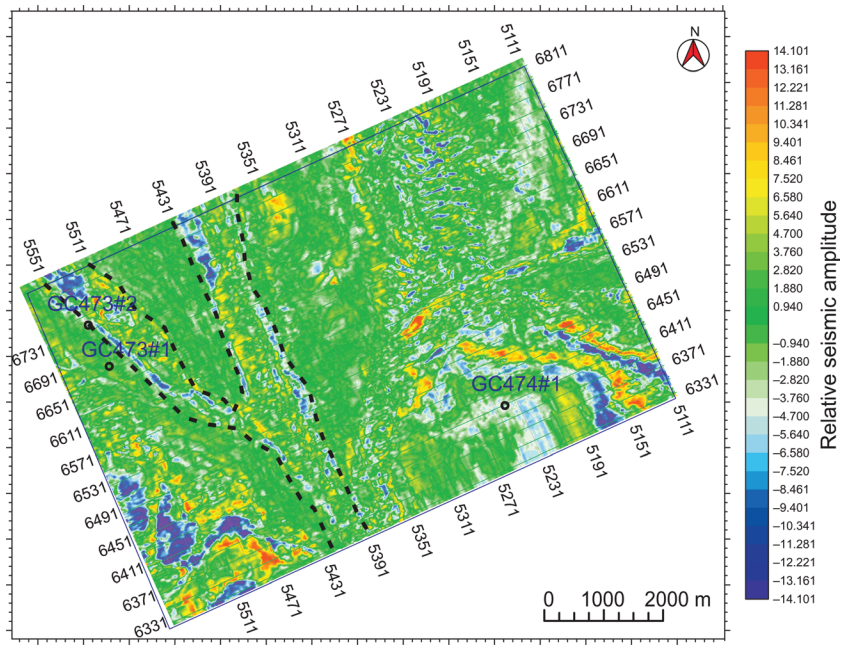

Figure 6. Map view of seismic amplitude at 0.4 s below seafloor. Dashed lines illustrate the interpreted channels.

equal to the total porosity of the sediments. The difference between these sediments is the gas hydrate and gas content in the pore space. When the water saturation decreases, resulting from gas hydrate filling the pore space, impedance increases. Therefore, we can see higher impedance in hydrate-saturated sediments than water-saturated sediments. Similarly, if free gas fills the pore space, both water saturation and impedance will decrease. We define the higher impedance as hydrate-associated impedance. The impedance ratio (the ratio of the hydrate associated impedance to the background impedance) will increase as gas hydrate saturation increases.

An effective medium rock physics model has been used to quantify gas hydrate saturation for high-porosity shallow sediments in the Outer Blake Ridge (Helgerud et al., 1999; Ecker et al., 2000), the Mackenzie Delta (Sakai, 1999), and the Gulf of Mexico (Xu et al., 2004). In Hertz-Mindlin contact theory, elastic bulk and shear moduli of the dry frame are described by assuming that the matrix consists of a random dense pack of elastic spherical grains that have normal and shear stiffness because of the grains contact. Saturated bulk modulus can then be calculated by Gassmann's fluid substitution. Velocity can be computed once saturated bulk modulus, shear modulus, and density are given. The fundamental principles of the rock physics model are presented by Mavko et al. (1998).

We use a three-phase model for hydrated-saturated sediments: matrix, fluid, and hydrate. First, we consider sediments without hydrate using the Hertz-Mindlin (Mindlin, 1949) contact theory and Gassmann's fluid substitution. Then, the hydrate effect can be expressed through the Hashin-Shtrikman (Hashin and Shtrikman, 1963) lower bound. Nur et al. (1998) interpret the Hashin-Shtrikman lower bound by using the critical porosity. When porosity is greater than the critical porosity, grains in sediment are mostly suspended; when porosity is less than the critical porosity, grains in sediment start to contact. Similarly, one of the main concerns regarding the gas hydrate rock-physics model is that the hydrate that generates in the pore space either acts as a component of the fluid, a component of the mineral frame, or both. Lee and Waite (2008) indicate that some hydrates act as fluid and other hydrates act as a mineral. They suggest a parameter (ε) of hydrate formation to describe the hydrate's effects on sediment stiffness. The parameter separates the two different behaviors that gas hydrates exhibit. If gas hydrate saturation is less than ε, saturated moduli are not affected significantly by gas hydrates. For the saturation greater than ε, the moduli increase obviously as saturation increases. Lab measurements (Yun et al., 2005) support the concept that few velocity changes occur in low hydrate saturation and large changes start from a hydrate saturation of 0.4. We use the parameter (ε) in the Hashin-Shtrikman lower bound.

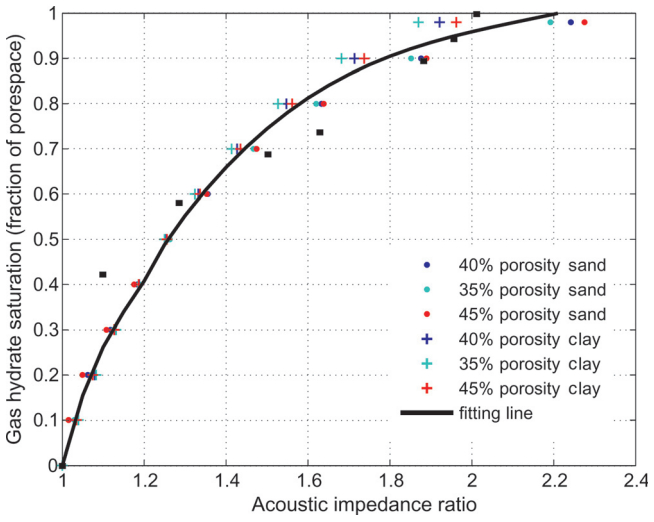

Figure 7. The relation between gas hydrate saturation and impedance ratio. The curve is fit to the rock physics model at 35%, 40%, and 45% porosity of sand and clay. The small black squares are lab measurements for 40% porosity of sand (Yun et al., 2005).

We use the model to calibrate a relation between the impedance ratio and gas hydrate saturation. Figure 7 shows the crossplot of the impedance ratio and gas hydrate saturation in the sands with $40 \pm 5\%$ and clays with $40 \pm 5\%$. In general, each sedimentological package in a sequence has an individual calibration. However, Figure 7 illustrates that the relationship for the shallow sediments are similar, except in very high gas hydrate saturation. For simplicity, a single relationship is applied to the whole study area.

Two populations mark two trends in Figure 7. The first population is composed of sands and clays with a gas hydrate saturation less than 0.5, defining the first trend; the second population is composed of those with a gas hydrate saturation greater than 0.5, defining the second trend. The slope is steeper in the first trend than the second one, indicating that the changes in lithology distribution and compaction state will more strongly affect gas-hydrate estimation in low saturated hydrated sediments. Sands and clays are dispersed in the second population, where the gas hydrate saturation is greater than 0.7. We suggest that gas hydrate estimation needs to be reevaluated in the postdrilling stage by combining seismic data with logging data.

Saturation and distribution of gas hydrate

The interpretation based on inverted acoustic impedance has more advantages than traditional amplitude interpretation in the study of gas hydrate. The acoustic impedance represents the physical characteristics of the lithology. Tuning effects are reduced because the wavelet is removed. Additional low frequencies integrated into acoustic impedance provide a full broadband solution. However, although the inversion algorithm has constrained the impedance trend and narrowed the range of possible solutions, seismic inversion theoretically offers nonunique solutions. Thus, the interpretation of acoustic impedance is important.

Figure 8 contains a final 2D acoustic impedance section. High acoustic impedance anomalies, interpreted to be gas hydrate, and low acoustic impedance anomalies, interpreted to be free gas, are observed within sand prone deposits in sequence 3, which is consistent with the amplitude interpretation. Prominent features in the figure are the high-over-low impedance layers, labeled H1, L1, and H2, and high-impedance bright spots, labeled S1, S2, and S3. These acoustic-impedance anomalies of layers (H1 and H2) cut by faults (faults B and C) in the southern part are shallower than those anomalies of spots (S1, S2, and S3) on the base of sequence 3 in the northern part. A possible explanation for the occurrence of gas hydrate at different depths is that the gas hydrate stability zone was moved upward

into a shallower section by thermal flow. The two features, interpreted as zones of highly concentrated hydrate, are similar to the bright spots (Hornbach et al., 2003) and lens (Hornbach et al., 2008) that were found in the Blake Ridge.

Acoustic impedance anomalies are present as layer distribution on both sides of the faults in the southern part of the study area (H1 and H2 in Figure 8). A similar phenomenon was found in JIP at GC955, about 55 km further south. Channel/levee sandy sediments close to the base of the gas hydrate stability zone are cut by faults. Highly concentrated gas hydrate is detected in sandy sediments from logging data in the GC955 H location (Guerin et al., 2009). Figure 8 illustrates an acoustic impedance range from 4.2 to 4.7 ($\times 10^6$ kg/m^3 $\times$ m/s) in the gas hydrate layers, higher than the normal background acoustic impedance of 3.5 to 3.9 ($\times 10^6$ kg/m^3 $\times$ m/s). This is similar to the observation made by vertical seismic profile (VSP) data in the lens in the Blake Ridge (Hornbach et al., 2008). The strength of the anomalies decreases away from the faults. The character of the acoustic impedance distribution suggests that the formation of highly concentrated gas hydrate needs enough gas accumulation. Gas is interpreted to migrate along the two buried faults (faults B and C in Figure 8).

The highly concentrated sheet-like gas hydrate consists of roughly north-south trending linear features on the plane view (Figure 9), covering about 0.9 km^2 of the study area. The presence of gas hydrate has a maximum concentration of approximately 0.2 of the sediment volume and a maximum saturation of approximately 0.5 of the pore space (Figure 10). We compute the average hydrate concentration of 0.2 by volume. Assuming the average vertical thickness of 20 m, the layers may contain 3.4×10^9 kg of gas hydrate.

High acoustic-impedance anomalies are present as spot distributions (S1, S2, and S3) in the northern part in Figure 8. The strength of the anomalies is weaker than those in the southern part (Figure 8). The presence of gas hydrate has a maximum concentration of approximately 0.15 of the sediment volume and a maximum saturation of approximately 0.4 of the pore space (Figure 10). The bright spots interpreted from impedance sections have lower gas hydrate saturation than those observed from amplitude waveform inversion in the Blake Ridge, where gas hydrate was estimated to be 50% to 70% of pore space within the bright spots (Hornbach et al., 2003).

The spot gas hydrate shows high variability in vertical and lateral distribution (Figures 9 and 10). The size of spot gas hydrate ranges from 50 m, or less, to 500 m in diameter (Figure 9). We estimate that spot gas hydrate covers 1% of the 60-km^2 study area and occurs in an average thickness of 15 m. Assuming an average hydrate concentration of 0.15 of volume, the total methane hydrate is estimated to be 1.3×10^9 kg. The lower saturation in the spot distribution compared to the layer distribution is discussed below.

DISCUSSION

Understanding and identifying gas hydrate systems from seismic data remains a challenge. Methane is stable as a solid under certain pressure and temperature conditions. However, in the Gulf of Mexico, gas hydrate occurs in a dynamic nonequilibrium system. The traditional gas hydrate indicators, BSRs and blanking zones, are not often observed from seismic data in the

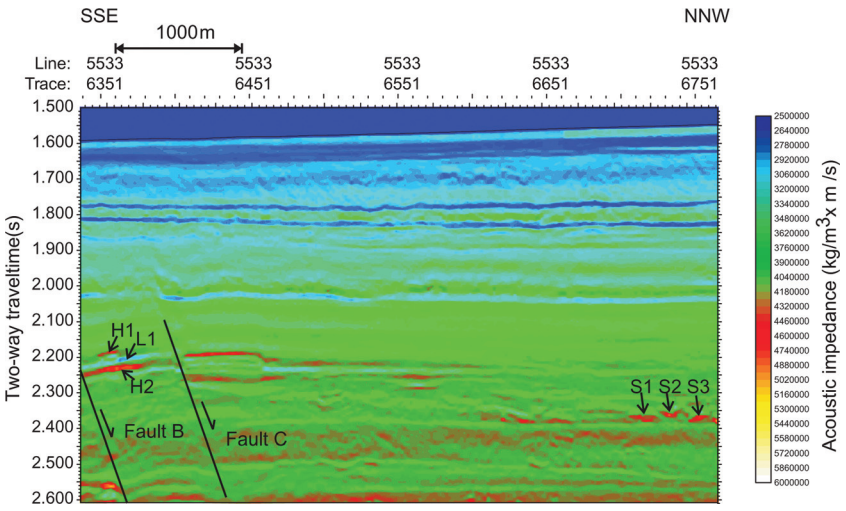

Figure 8. Inverted acoustic impedance inline 5533 from 3D seismic data. L1 is a low-impedance layer. H1 and H2 are two high impedance layers. S1, S2 and S3 are high-impedance bright spots.

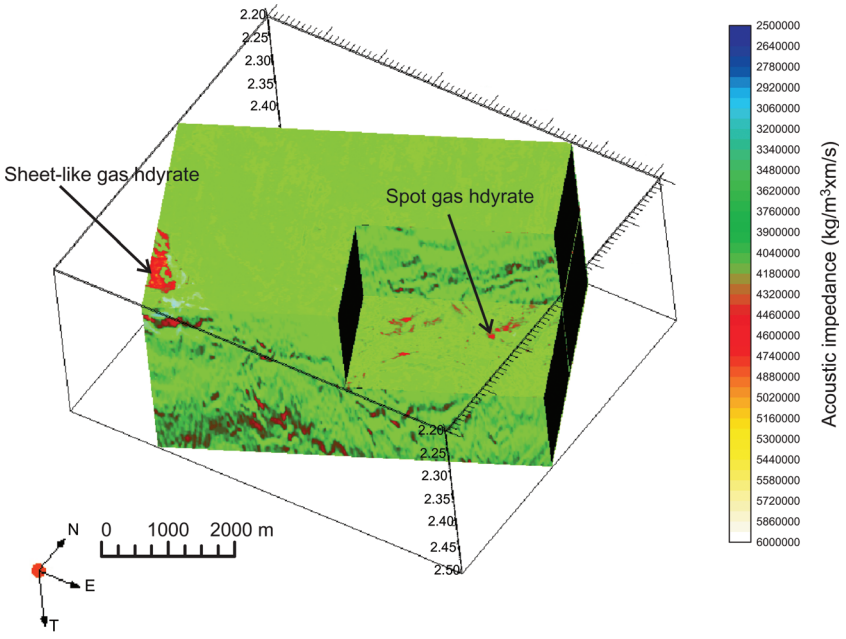

Figure 9. Various slices through 3D acoustic impedance volume show sheet-like gas hydrate and spot gas hydrate.

system. We investigate gas hydrate formation, migration, and accumulation, as well as new gas hydrate indicators.

Faulting and sand and fluid flow

Fluid flow plays an important role in the formation of gas hydrate. A fault may provide a pathway for the migration of fluid to form gas hydrate above the gas hydrate stability zone (Rowe and Gettrust, 1993). In hydrodynamic environments, although gas usually moves vertically upward due to buoyancy, water may move in any direction. Thus, fluid (including both water and gas) migration can be vertical along faults, which act as pathways for fluid transport; it also can be horizontal within high permeability sandy sediments, where water potential is not zero. The sandy sediments may act as either pathways or intermediate reservoirs to concentrate fluids (Gay et al., 2007). Cooper and Hart (2002) illustrate that fluid/gas migrates upward along faults extending to the seafloor and moves into reservoir sand to form gas hydrate in a fault-flow model.

A large fault (fault A in Figure 4) deeply cuts low-saturation gas sands in approximately 3430 m BSS in the vicinity of well GC474 #1 (O'Brien, 2004). O'Brien indicates that gas has escaped from the sand bodies in the dynamic system due to the absence of a gas cap, which is consistent with these seafloor mounds along the large fault (Figures 1 and 5). These mounds are interpreted to be fluid expulsion features (Figure 11). Our result shows only a small amount of accumulation of gas hydrate within the gas hydrate stability zone in the subsurface area near the fault (Figure 10). The phenomenon may be caused by high heat flow and/or high-salinity fluids if the fluid migration is active or rent active (Roberts et al., 2006). The base of the gas hydrate stability zone rises to the seafloor with the rapid fluid gas expulsion. Another possible explanation is that the fault is a sealing fault in most of the area so little free gas can move horizontally into sandy sediments to form gas hydrate within the gas hydrate stability zone.

A fault zone with two buried faults (faults B and C in Figure 4) cuts high-saturation gas sand in deep section in the vicinity of the well GC473 #1 (O'Brien, 2004). Gas may migrate into the shallow section along the fault zone. The overlying fine-grained clay with low permeability above the fault zone acts as a barrier (sequence 2 in Figure 4). The barrier to migration results in gas horizontally advecting into sandy sediments and accumulating within the sediments. Our result shows a high accumulation of gas hydrate near the top of the buried faults in the sandy sediments within the gas hydrate stability zone (Figure 10). Figure 8 shows where the buried faults cut the high concentration gas hydrate layers (H1 and H2). The migration flux is interpreted to be slower than in the area of the large accurate faults (Figure 11). The temperature and salinity are moderate, so gas hydrate can accumulate in the subsurface.

No obvious faults are found in the area of spot gas hydrate (S1, S2, and S3 in Figures 8 and 9). Fluid migration is interpreted to be caused by buoyancy and water flow. Fluid moves laterally along strata boundaries and moves vertically in permeable heterogeneities in clays and accumulates in the fractures or separate sand bodies (Figure 11). Gas may also pass vertically through fine-grained sedimentary sections by diffusion (Cooper and Hart, 2002).

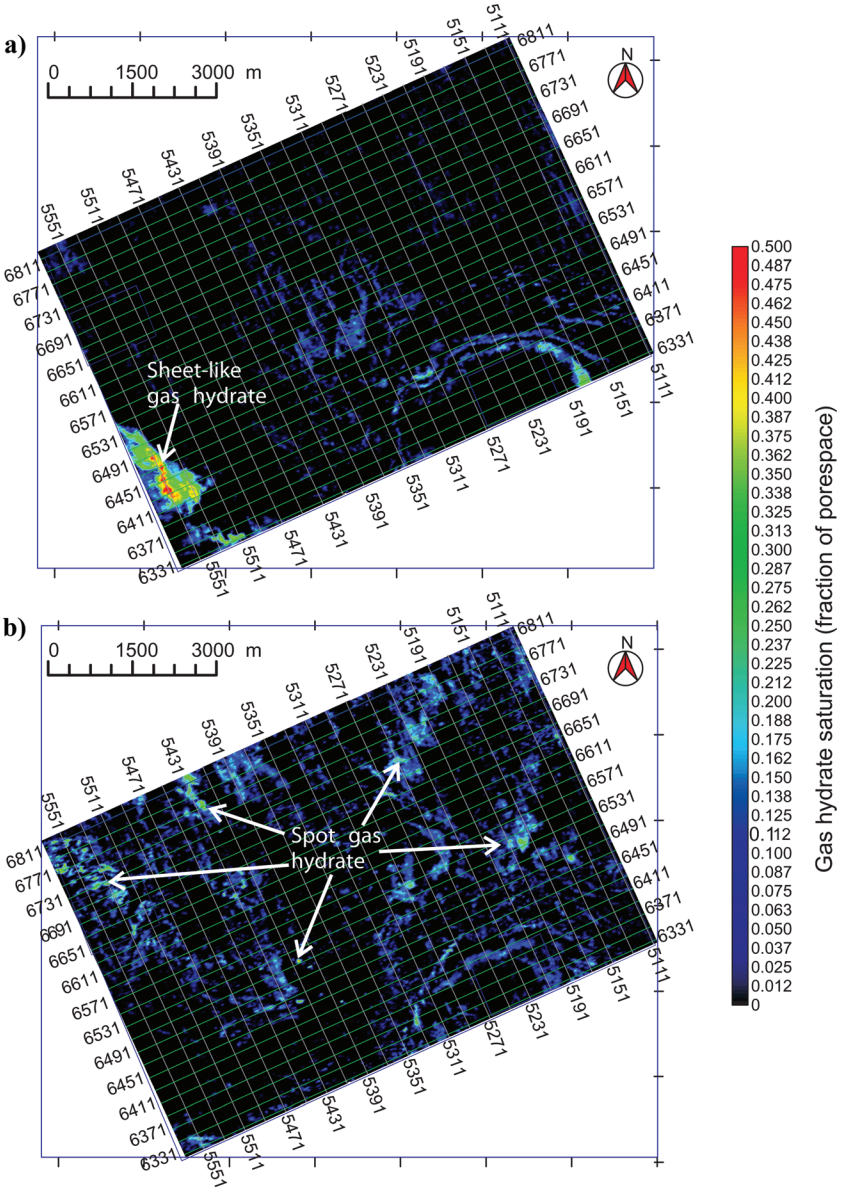

Figure 10. Slices show the predicted gas hydrate saturation 0.61 s below seafloor (a) and 0.78 s below seafloor (b).

Presence of free gas within the gas hydrate stability zone

Free gas has been found within the gas hydrate stability zone at the southern summit of Hydrate Ridge (Milkov et al., 2004; Torres

et al., 2004), Black Ridge (Gorman et al., 2002), and offshore Peru (Netzeband et al., 2005). The interbed between gas hydrate layers H1, H2, and free gas layer L1 (Figure 8) suggests the possibility that free gas exists within the gas hydrate stability zone in our study area.

The possible reasons for the occurrence of free gas within the gas hydrate stability zone could include the source of gas, the kinetics of gas hydrate formation, and overpressure caused by high methane flux. The structure II thermogenic gas hydrate, which includes more ethane, propane, and isobutane than structure I methane gas hydrate, is abundant in the Green Canyon and was found in GC185 (Sassen et al., 1999a) and GC232 (Orcutt et al., 2004). The structure II gas hydrate can form at lower pressures and higher temperatures than the structure I gas hydrate (Sloan, 1998). Gas hydrate is not stable under relative high fluid flux due to high-saline brines (Milkov et al., 2004) and heat (Ruppel et al., 2005) as a result of hydrate formation. Hydrate, water, and free gas may not reach the thermodynamic equilibrium in this case. Xu and Ruppel (1999) predict that methane flux into the gas hydrate stability zone has to exceed a critical methane flux to have free gas and gas hydrate coincide at the base of the hydrate stability zone. A trapped free gas accumulation under gas hydrate may lead to overpressure that can open fractures or activate preexisting faults, so that gas quickly migrates upwards along the fractures or preexisting faults (Flemings et al., 2003). Our study generally fits these models. Free gas interpreted to be within the gas hydrate layers indicates that the fluid flow is currently active. Gas would be associated with a commercial gas reservoir in the deep section, which is leaking from the reservoir and migrating into the shallow section.

The coexistence of free gas and gas hydrate would be a local variation of hydrate stability in a small-scale area. We do not consider the coexistence in the microstructure rock physics model. High P-impedance indicates highly concentrated gas hydrate, and low P-impedance indicates free gas in the study area. Both impedance anomalies can generate amplitude anomalies in the seismic reflection section.

BSR and the gas hydrate stability zone

The classic BSR is not recognized from 3D seismic data in our study area. Different mechanisms have been proposed for the absence of BSR in the Gulf of Mexico. In general, insufficient gas hydrate and free gas at the base of the gas hydrate stability zone cause BSR to be absent. We interpret three reasons for the absence of the BSR in the area. The first reason is the sources of gas. Thermogenic gas originating from the deep sections is abundant in the study area, but microbial gas generated in situ is deficient. The second reason may be different fluid flux acting on different sediments. The shallow geology is complex (Figure 4), in contrast to the clay-rich uniform deposits in the Black Ridge. The observations of the seafloor expulsion features along the arcuate fault and highly concentrated gas hydrate in the top of the buried faults suggest focused fluid flow in the area (Figure 11). Only little diffuse fluid flow with dissolved gas moves vertically through the sedimentary layers (Figure 11). Thus, there is not enough dissolved gas to exceed the critical methane rate in the area. Highly concentrated gas hydrate and the free gas zone below it are difficult to form in the clay sediments. Another possible reason is that the rapid sedimentation rates cause the gas hydrate stability zone to quickly migrate upward. Submarine landslide deposits in sequences 1 and 2 indicate rapid deposition in the area. Dissolved gas toward the seafloor moves too slowly to accumulate hydrate and free gas in the clay sediments.

Although BSRs are difficult to form in the clay in the Gulf of Mexico, the highly concentrated gas hydrates are possibly found in the sandy sediments. We suggest that high amplitude and high-impedance anomalies may be hydrate indicators. These anomalies are more likely to represent as local and scattered features within the gas hydrate stability zone and may vary laterally with depth in the dynamic nonequilibrium gas hydrate system in the Gulf of Mexico. Both amplitude and impedance anomalies in sand deposits are found in the area (H1, H2, S1, S2, and S3 in Figure 8). The interpreted anomalies are located within the sand-prone sediments in the western part of the study area (Figures 8 and 9). Unlike other interpreted BSRs that truncate the lithologies, the anomalies consist of several bright spots aligning with the seafloor (S1, S2, and S3 in Figure 8). The interpreted anomalies (H1 and H2 in Figure 8) are shallow in the southwest because the base of the gas hydrate stability zone moves upward due to the relatively high fluid flux (Figure 11). The anomalies disappear in the eastern area, where the sand-prone sediments are deeper than the base of the gas hydrate stability zone.

Accuracy of hydrate saturation

We estimate the gas hydrate saturation based on seismic inversion and a rock physics transform. As with any seismic inversion, seismic data quality and ambiguities associated with the inversion affect the accuracy of the impedance. We deal carefully with the wavelet and the initial geological model to minimize the ambiguities during the inversion. Highly concentrated hydrate sediments and gassy sediments provide enough

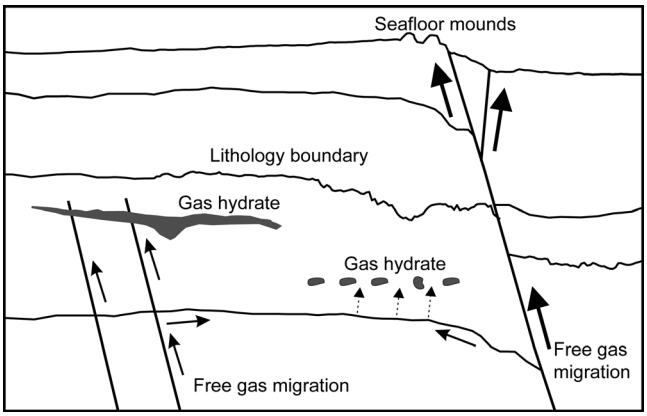

Figure 11. Geological interpretation of the expected fluid flow system and relation to gas hydrate formation. The rapid fluid system transports fluid and gas along the seafloor faults, creating seafloor mounds. Fluid and gas migrate along the buried fault and generate layer gas hydrate in the moderate fluid system. The slow fluid system transports them along the lithology boundaries or high permeability lithologic layers generating spot gas hydrate. Thick solid arrows, rapid fluid flux; thin solid arrows, moderate fluid flux; dashed arrows, slow fluid flux.

impedance contrast to allow separation from nonhydrate or nongas sediments. Thus, estimated acoustic impedance is a viable tool to identify highly concentrated gas hydrate and free gas.

The accuracy of the hydrate saturation is also dependent on the gas hydrate rock physics model and the rock physics depth trend. We assumed an average trend of clays as a background. All estimated acoustic impedances above the background are expected to be caused by gas hydrate occupying the pore space of the sediments. No elder lithology extrudes into the shallow sections in our study area; sequences 1, 2, and 3 were interpreted to be under the relative normal compaction. However, local subsequences could have high-acoustic impedance because of local geologic complexity. On the other hand, the gas hydrate rock physics model has not been calibrated by in situ logging data or laboratory measurements. Thus, the value of predicted hydrate saturation may not represent realistic gas hydrate concentration; however, high-hydrate saturation indeed indicates the potential for gas hydrate occurrence within sediments.

The estimated hydrate saturation provides additional information to assess potential drilling location for gas hydrate exploration, while it will be revised from the result of postdrilling. We recommend that the prestack seismic inversion be considered in areas of highly concentrated gas hydrate when developing a drilling plan for gas hydrate exploration wells in the area. A P-impedance anomaly associated with an S-impedance anomaly would offer further confidence for the presence of gas hydrate.

CONCLUSIONS

We have qualitatively interpreted seafloor features, subsurface faults, and seismic sequences from seismic reflection data. The occurrence of highly concentrated gas hydrate is interpreted to be in the sand-prone deposits in sequence 3. Seismic acoustic inversion and a rock physics model transform provide quantitative interpretability and improve the interpretation of sand-prone gas hydrate deposits in the area. Seismic acoustic inversion can provide quantitative interpretation for low impedance, which can be representative of gas sands, and high impedance, which can be representative of hydrate sands. The rock physics model transform can quantitatively interpret the concentration of gas hydrate and map its distribution. Integrating both qualitative and quantitative interpretation provides a better tool for gas hydrate interpretation.

In our study area, gas hydrate is estimated to have a concentration of up to 0.2 by volume. Highly concentrated gas hydrate is interpreted to be present as a layer distribution in 2D or a sheet-like distribution in 3D data in the southwestern part of the study area and present as spot distribution in other areas. Gas is coexists with gas hydrate.

We observe the evidence that highly concentrated gas hydrates are associated with underlying structures (seafloor faults, buried faults, and salt) and stratigraphy (sand-prone deposits) in the study area. Fluid migrates both vertically along the faults and laterally within sand-prone sediments and sediment boundaries. Free gas accumulates within the sand-prone sediments to form highly concentrated gas hydrate in the low to moderate fluid flux environment, whereas highly concentrated gas hydrate does not occur within the same sequence in the high fluid flux environment. Scattered gas hydrate in discontinuous sand bodies forms from the low fluid flux or when dissolved gas exceeding the critical rate in the dynamic gas hydrate system.

Traditional gas hydrate indicators, classic BSRs and blanking zones, are not found in the study area. A number of high amplitude anomalies within sand-prone sediments are associated with high acoustic impedance caused by highly concentrated gas hydrate and low acoustic impedance caused by free gas. These amplitude and impedance anomalies, located in the base of the hydrate stability zone and close to the fluid flow zone, may be considered as gas hydrate indicators.

ACKNOWLEDGMENTS

We thank WesternGeco for providing seismic data to the University of Houston. We thank Anadarko for assisting the University of Houston to gain access to the data. We thank Hampson-Russell for the STRARA inversion software package. We appreciate the perceptive comments of three anonymous reviewers and the associate editor. We appreciate Tommy Ringo of University of Houston, who edited the manuscript and made it much more readable. We also gratefully acknowledge Dan McConnell, Timothy Collett, and Patrick Hart for comments on this manuscript.

REFERENCES

Abrams, M. A., 1992, Geophysical and geochemical evidence for subsurface hydrocarbon leakage in the Bering Sea, Alaska: Marine and Petroleum Geology, **9**, no. 2, 208–221, doi:10.1016/0264-8172(92)90092-S.

Andreassen, K., P. E. Hart, and A. Grantz, 1995, Seismic studies of a bottom-simulating refection related to gas hydrates beneath the continental margin of the Beaufort Sea: Journal of Geophysical Research, **100**, 12659–12673, doi:10.1029/95JB00961.

Andreassen, K., P. E. Hart, and M. Mackay, 1997, Amplitude versus offset modeling of the bottom simulating reflection associated with submarine gas hydrates: Marine Geology, **137**, no. 1–2, 25–40, doi:10.1016/S0025-3227(96)00076-X.

BOEMRE (Bureau of Ocean Energy Management, Regulation and Enforcement), 2010, Safety performance review — Shallow waterflows can pose significant hazards to deepwater drilling: http://www.gomr.boemre.gov/homepg/offshore/safety/waterflow/wtrflow.html.

Boswell, R., T. S. Collett, M. Frye, D. McConnell, W. Shedd, S. Mrozewski, G. Guerin, and A. Cook, 2009, Gulf of Mexico Gas Hydrate Joint Industry Project Leg II — Technical summary: Proceedings of the drilling and scientific results of the 2009 Gulf of Mexico Gas Hydrate Joint Industry Project Leg II, http://www.netl.doe.gov/technologies/oil-gas/publications/Hydrates/2009Reports/TechSum.pdf.

Brooks, J. M., M. C. Kennicutt II, R. R. Fay, T. J. McDonald, and R. Sassen, 1984, Thermogenic gas hydrates in the Gulf of Mexico: Science, **225**, 409–411, doi:10.1126/science.225.4660.409.

Brown, A., 2000, Evaluation of possible gas microseepage mechanisms: The AAPG Bulletin, **84**, 1775–1789.

Cooper, A. K., and P. E. Hart, 2002, High-resolution seismic-reflection investigation of the northern Gulf of Mexico gas-hydrate-stability zone: Marine and Petroleum Geology, **19**, 1275–1293, doi:10.1016/S0264-8172(02)00107-1.

Dallimore, S. R., T. Uchida, and T. S. Collett, 1999, Scientific results from JAPEX/JNOC/GSC Mallik 2L-38 gas hydrate research well, Mackenzie Delta, Northwest Territories, Canada: Geological Survey of Canada Bulletin, 544.

Dev, A., and G. A. McMechan, 2010, Interpreting structural controls on hydrate and free-gas accumulation using well and seismic information from the Gulf of Mexico: Geophysics, **75**, no. 1, B35–B46, doi:10.1190/1.3282680.

Dutta, T., 2009, Integrating sequence stratigraphy and rock-physics to interpret seismic amplitudes and predict reservoir quality: Ph.D. thesis, Stanford University.

Ecker, C., J. Dvorkin, and A. Nur, 1998, Sediments with gas hydrates: Internal structure from seismic AVO: Geophysics, **63**, 1659–1669, doi:10.1190/1.1444462.

———, 2000, Estimating the amount of gas hydrate and free gas from marine seismic data: Geophysics, **65**, 565–573, doi:10.1190/1.1444752.

Expedition 311 Scientists, 2006, Expedition 311 summary, *in* Riedel, M., T. S. Collett, M. J. Malone, and the Expedition 311 Scientists. Proceedings of the IODP, 311: Washington, DC (Integrated Ocean Drilling Program Management International, Inc.), doi:10.2204/iodp.proc.311.101.2006.

Flemings, P. B., X. Liu, and W. J. Winters, 2003, Critical pressure and multiphase flow in Blake Ridge gas hydrates: Geology, **31**, 1057–1060, doi:10.1130/G19863.1.

Forrest, J., E. Marcucci, and P. Scott, 2005, Geothermal gradients and subsurface temperatures in the Northern Gulf of Mexico: GCAGS Transactions, **55**, 233–248.

Gay, A., M. Lopez, C. Berndt, and M. Seranne, 2007, Geological controls on focused fluid flow associated with seafloor seeps in the Lower Congo Basin: Marine Geology, **244**, no. 1-4, 68–92, doi:10.1016/j.margeo.2007.06.003.

Gorman, A. R., W. S. Holbrook, M. J. Hornbach, K. L. Hackwith, D. Lizarralde, and I. Pecher, 2002, Migration of methane gas through the hydrate stability zone in a low-flux hydrate province: Geology, **30**, 327–330, doi:10.1130/0091-7613(2002)030<0327:MOMGTT>2.0.CO;2.

Gregory, A. R., 1977, Aspects of rock physics from laboratory and log data that are important to seismic interpretation, *in* Payton, C.E. ed., Seismic stratigraphy — Applications to hydrocarbon exploration: AAPG Memoir, **26**, 15–46.

Guerin, G., A. Cook, S. Mrozewski, T. S. Collett, and R. Boswell, 2009, Gulf of Mexico Gas Hydrate Joint Industry Project Leg II — Green Canyon 955 LWD operations and results: Proceedings of the Drilling and Scientific Results of the 2009 Gulf of Mexico Gas Hydrate Joint Industry Project Leg II. http://www.netl.doe.gov/technologies/oil-gas/publications/Hydrates/2009Reports/GC 955LWDOps/pdf.

Hamilton, E. L., 1979, Vp/Vs and Poisson's ratio in marine sediments and rocks: Journal of the Acoustical Society of America, **66**, 1093–1101.

Hashin, Z., and Shtrikman, S., 1963. A variational approach to the theory of the elastic behaviour of multiphase materials. Journal of Mechanics and Physics of Solids, **11**, 127–140.

Helgerud, M. B., J. Dvorkin, A. Nur, A. Sakai, and T. S. Collett, 1999, Elastic-wave velocity in marine sediments with gas hydrates: Effective medium modeling: Geophysical Research Letters, **26**, 2021–2024, doi:10.1029/1999GL900421.

Hornbach, M. J., W. S. Holbrook, A. R. Gorman, K. L. Hackwith, D. Lizarralde, and I. Pecher, 2003, Direct seismic detection of methane hydrate on the Blake Ridge: Geophysics, **68**, 92–100, doi:10.1190/1.1543196.

Hornbach, M. J., D. M. Saffer, W. S. Holbrook, H. J.A. Van Avendonk, and A. R. Gorman, 2008, Three-dimensional seismic imaging of the Blake Ridge methane hydrate province: Evidence for large, concentrated zones of gas hydrate and morphologically driven advection: Journal of Geophysical Research, **113**, B07101–B07115, doi:10.1029/2007JB005392.

Hutchinson, D. R., D. Shelander, J. Dai, D. McConnell, W. Shedd, M. Frye, C. Ruppel, R. Boswell, E. Jones, T. Collett, K. Rose, B. Dugan, W. Wood, and T. Latham, 2008, Site selection for DOE/JIP gas hydrate drilling in the northern Gulf of Mexico: Sixth International Conference on Gas Hydrates, https://circle.ubc.ca//handle/2429/1165.

Jones, E., T. Latham, D. McConnell, and M. Frye Jr., J. Hunt, W. Shedd, D. Shelander, R. Boswell, K. Rose, C. Ruppel, D. Hutchinson, T. Collett, B. W. Dugan, and W. Wood, 2008, Scientific objectives of the Gulf of Mexico gas hydrate JIP Leg II drilling: Presented at the Offshore Technology Conference, http://www.boemre.gov/revaldiv/PDFs/HydratesPub-OTC.pdf.

Kvenvolden, K. A., 1998, A primer on the geological occurrence of gas hydrates, *in* J. P. Henriet and J. Mienert, eds., Gas hydrates-relevance to world margin stability and climatic change: Geological Society of London Special Publications 137, 9–30, doi: 10.1144/GSL.SP.1998.137.01.02.

Kvenvolden, K. A., and L. A. Barnard, 1982, Hydrates of natural gas in continental margins, *in* J. S. Watkins and C. L. Drake, eds., Studies in continental margin geology: AAPG Memoir 34, 631–640.

Lee, M. W., and W. F. Waite, 2008, Estimating pore-space gas hydrate saturations from well log acoustic data: Geochemistry Geophysics Geosystems, **9**, Q07008–Q07015, doi:10.1029/2008GC002081.

Li, Q., 2001, LP sparse spike inversion, Strata technique document: Hampson-Russell Software Services Ltd.

Lu, S., and G. A. McMechan, 2002, Estimation of gas hydrate and free gas saturation, concentration, and distribution from seismic data: Geophysics, **67**, 582–593, doi:10.1190/1.1468619.

MacDonald, I. R., G. S. Boland, J. S. Baker, J. M. Brooks, and M. C. Kennicutt, 1989, Gulf of Mexico hydrocarbon seep communities II. Spatial distribution of seep organisms and hydrocarbons at Bush Hill: Marine Biology, **101**, 235–247.

Mann, R. G., W. R. Bryant, and P. D. Rabinowitz, 1992, Seismic facies interpretation of the northern Green Canyon area, Gulf of Mexico, *in* J. S. Watkins, F. Zhiqiangm, and K. J. McMillen, eds., Geology and geophysics of continental margins: AAPG Memoir 53, 343–360.

Markl, R. G., G. M. Bryan, and J. I. Ewing, 1970, Structure of the Blake-Bahama outer ridge: Journal of Geophysical Research, **75**, 4539–4555, doi:10.1029/JC075i024p04539.

Mavko, G., T. Mukerji, and J. Dvorkin, 1998, Rock physics handbook: Tools for seismic analysis in porous media: Cambridge University Press.

McConnell, D., and B. Kendall, 2002, Images of the base of gas hydrate stability, Northwest Walker Ridge, Gulf of Mexico: Presented at the Offshore Technology Conference.

Milkov, A. V., G. R. Dickens, G. E. Claypool, Y.-J. Lee, W. S. Borowski, M. E. Torres, W. Xu, H. Tomaru, A. M. Tréhu, and P. Schultheiss, 2004, Co-existence of gas hydrate, free gas, and brine within the regional gas hydrate stability zone at Hydrate Ridge (Oregon margin): Evidence from prolonged degassing of a pressurized core: Earth and Planetary Science Letters, **222**, 829–843, doi:10.1016/j.epsl.2004.03.028.

Milkov, A. V., and R. Sassen, 2002, Economic geology of offshore gas hydrate accumulations and provinces: Marine and Petroleum Geology, **19**, 1–11, doi:10.1016/S0264-8172(01)00047-2.

Mindlin, R. D., 1949, Compliance of elastic bodies in contact: Journal of Applied Mechanics, **16**, 259–268.

Netzeband, G. L., C. P. Hübscher, D. Gajewski, J. W. G. Grobys, and J. Bialas, 2005, Seismic velocities from the Yaquina forearc basin off Peru: Evidence for free gas within the gas hydrate stability zone: International Journal of Earth Sciences, **94**, 420–432, doi:10.1007/s00531-005-0483-2.

Nur, A., G. Mavko, J. Dvorkin, and D. Galmudi, 1998, Critical porosity:A key to relating physical properties to porosity in rocks: The Leading Edge, **17**, 357–362, doi:10.1190/1.1437977.

O'Brien, J., 2004, Seismic amplitude from low gas saturation sands: The Leading Edge, **23**, 1236–1243. doi:10.1190/1.1843380

Orcutt, B. N., A. Boetius, S. K. Lugo, I. R. MacDonald, V. A. Samarkin, and S. B. Joye, 2004, Life at the edge of methane ice: Microbial cycling of carbon and sulfur in Gulf of Mexico gas hydrates: Chemical Geology, **205**, no. 3-4, 239–251, doi:10.1016/j.chemgeo.2003.12.020.

Ostermeier, R. M., J. H. Pelletier, C. D. Winker, J. W. Nicholson, F. H. Rambow, and C. K. Cowan, 2002, Dealing with shallow-water flow in the deepwater Gulf of Mexico: The Leading Edge, **21**, 662–668, doi:10.1190/1.1497320.

Pflaum, R. C., J. M. Brooks, H. B. Cox, M.C. Kennicutt II, and D. D. Sheu, 1986, Molecular and isotopic analysis of core gases and gas hydrates, Deep Sea Drilling Project Leg 86, *in* A. H. Bouma, J. M. Coleman, and A. W. Meyer, et al., Initial reports of the Deep Sea Drilling Project: U. S. Government Printing Office, vol. 96, 781–784.

Reilly, J. F. Jr., I. R. MacDonald, E. K. Biegert, and J. M. Brooks, 1996, Geologic controls on the distribution of chemosynthetic communities in the Gulf of Mexico, *in* D. Schumacher and M. A. Abrams, eds., Hydrocarbon migration and its near-surface expression: AAPG Memoir 66, 39–62.

Roberts, H. H., B. A. Hardage, W. W. Shedd, and J. Hunt Jr., 2006, Seafloor reflectivity — An important seismic property for interpreting fluid/gas expulsion geology and the presence of gas hydrate: The Leading Edge, **25**, 620–628, doi:10.1190/1.2202667.

Rowe, M. M., and J. F. Gettrust, 1993, Faulted structure of the bottom-simulating reflector on the Blake Ridge, western North Atlantic: Geology, **21**, 833–836, doi:10.1130/0091-7613(1993)021<0833:FSOTBS>2.3.CO;2.

Ruppel, C., R. Boswell, and E. Jones, 2008, Scientific results from Gulf of Mexico gas hydrates joint industry project Leg I drilling: Introduction and overview: Marine and Petroleum Geology, **25**, 819–829, doi:10.1016/j.marpetgeo.2008.02.007.

Ruppel, C., G. R. Dickens, D. G. Castellini, W. Gilhooly, and D. Lizarralde, 2005, Heat and salt inhibition of gas hydrate formation in the northern Gulf of Mexico: Geophysical Research Letters, **32**, L04605–L04608, doi:10.1029/2004GL021909.

Sakai, A., 1999, Velocity analysis of vertical seismic profile (VSP) survey at JAPEX/JNOC/GSC Mallik 2L-38 gas hydrate research well, and related problems for estimating gas hydrate concentration: Bulletin — Geological Survey of Canada, Report 544, 323–340.

Sassen, R., S. T. Sweet, A. V. Milkov, D. A. DeFreitas, and M.C. Kennicutt II, 2001, Thermogenic vent gas and gas hydrate in the Gulf of Mexico slope:Is gas hydrate decomposition significant?: Geology, **29**, 107–110, doi:10.1130/0091-7613(2001)029<0107:TVGAGH>2.0.CO;2.

Sassen, R., S. T. Sweet, A. V. Milkov, D. A. DeFreitas, G. G. Salata, and E. C. McDade, 1999a, Geology and geochemistry of gas hydrates, central Gulf of Mexico continental slope: Gulf Coast Association of Geological Societies Transactions, **49**, 462–468.

———, 1999b, Thermogenic gas hydrate and hydrocarbon gases in complex chemosynthetic communities, Gulf of Mexico continental slope: Organic Geochemistry, **30**, 485–497, doi:10.1016/S0146-6380(99)00050-9.

Sloan, E. D., 1998, Clathrate hydrate of natural gas, 2nd ed.:Marcel Dekker.

Tréhu, A. M., P. E. Long, M. E. Torres, G. Bohrmann, F. R. Rack, T. S. Collett, D. S. Goldberg, A. V. Milkov, M. Riedel, P. Schultheiss, N. L. Bangs, S. R. Barr, W. S. Borowski, G. E. Claypool, M. E. Delwiche, G. R. Dickens, E. Gracia, G. Guerin, M. Holland, J. E. Johnson, Y.-J. Lee, C.-S. Liu, X. Su, B. Teichert, H. Tomaru, M. Vanneste, M. Watanabe, and J. L. Weinberger, 2004, Three-dimensional distribution of gas hydrate beneath southern Hydrate Ridge: Constraints from ODP Leg 204: Earth and Planetary Science Letters, **222**, 845–862, doi:10.1016/j.epsl.2004.03.035.

Torres, M. E., K. Wallmann, A. M. Tréhu, G. Bohrmann, W. S. Borowski, and H. Tomaru, 2004, Gas hydrate growth, methane transport, and chloride enrichment at the southern summit of Hydrate Ridge, Cascadia margin off Oregon: Earth and Planetary Science Letters, **226**, 225–241, doi:10.1016/j.epsl.2004.07.029.

Xu, H., J. Dai, F. Snyder, and N. Dutta, 2004, Seismic detection and quantification of gas hydrates using rock physics and seismic inversion, *in* C. Taylor and J. Kwan, eds., Advances in the study of gas hydrates: Kluwer Academic/Plenum Publishers, 117–139.

Xu, W., and C. Ruppel, 1999, Predicting the occurrence, distribution, and evolution of methane gas hydrate in porous marine sediments: Journal of Geophysical Research, **104**, 5081–5095, doi:10.1029/1998JB900092.

Yuan, T., R. D. Hyndman, G. D. Spence, and B. Desmons, 1996, Seismic velocity increase and deep-sea gas hydrate concentration above a bottom-simulating reflector on the northern Cascadia continental slope: Journal of Geophysical Research, **101**, 13655–13671, doi:10.1029/96JB00102.

Yuan, T., G. D. Spence, R. D. Hyndman, T. A. Minshull, and S. C. Singh, 1999, Seismic velocity studies of a gas hydrate bottom simulating reflector on the northern Cascadia continental margin: Amplitude modeling and full waveform inversion: Journal of Geophysical Research, **104**, 1179–1191, doi:10.1029/1998JB900020.

Yun, T. S., F. M. Francisca, J. C. Santamarina, and C. Ruppel, 2005, Compressional and shear wave velocities in uncemented sediment containing gas hydrate: Geophysical Research Letters, **32**, L10609–L10613, doi:10.1029/2005GL022607.

Zhang, Z., and G. A. McMechan, 2006, Elastic inversion for distribution of gas hydrate, with emphasis on structural controls: Journal of Seismic Exploration, **14**, 349–370.